

ms. 15 Feb. 2002

## **Transition Zone Structure Under the Northern North Sea**

George Helffrich

Earth Sciences, University of Bristol, Bristol, UK

Eugenio Asencio, James Knapp and Tom Owens

Geological Science, University of South Carolina, Columbia, SC 29208, USA

### **Abstract**

We report results from a year-long deployment of broadband seismometers in Scotland to study the mantle structure in the northern United Kingdom. The region is tectonically inactive and its underlying transition zone should not show unusual structure due to thermal perturbations caused by Cenozoic subduction or plume-related volcanism. The estimated 410- and 660-km discontinuity depths, estimated by receiver function stacking, are  $414 \pm 5$  and  $655 \pm 14$  km, average world-wide values. There is no evidence for a discontinuity at 520 km. The 660-km discontinuity conversion is weaker than global earth models predict by factors of  $1.05 - \sim 3$  within amplitude measurement uncertainties. Either significant attenuation below 410 km or regional, non-thermal variations in 660 properties that decrease its velocity and density jumps to  $1.9\% \Delta V_p$ ,  $4.8\% \Delta V_s$ , and  $4.8\% \Delta \rho$ , or that or broaden it to 13-35 km width could account for the lower than expected amplitudes. Lateral variations in transition zone water content around the 660-km discontinuity may be responsible for the broadening.

## Introduction

The transition zone discontinuities at 410 and 660 km are generally attributed to phase transitions in mantle minerals, principally in the  $(\text{Mg,Fe})_2\text{SiO}_4$  component of mantle peridotite [Bina and Wood, 1987; Ita and Stixrude, 1992; Helffrich, 2000]. On this account, the discontinuity properties respond to changes in temperature and potentially composition in the mantle by changing their depths and sharpness. While the influence of temperature on discontinuity position is fairly well-established (see discussion in Helffrich [2000]), the evidence for chemical influence is not as convincing but growing [Simmons and Gurrola, 2000; Deuss and Woodhouse, 2001]. Two sources of doubt are uncertainty over what chemical differences should exist in the transition zone (and thus what any discontinuity response should be), and the unmodeled effects of topography on the discontinuity surface. Topography is nettlesome because small-scale roughening of the surface can extinguish P-to-S conversions from a discontinuity [van der Lee *et al.*, 1994]. Thus, in order to explore the effect of chemistry on discontinuity structure, areas must be sought which are as free of extraneous influences as feasible.

Tectonically old areas provide useful study localities for this reason. By definition they do not overlie active subduction, the strongest thermal perturbation that can be envisaged in the upper mantle. Nor do they contain active volcanic provinces, either related to rifting or mid-plate volcanism, both of which affect the thermal profile of the shallow mantle [White and McKenzie, 1989]. Thus thermal effects are minimized. One such area is the United Kingdom, whose last significant tectonic episode took place in the early Tertiary ( $\sim 60$  Ma), when the rifting that led to the formation of the Atlantic Ocean began [Harris, 1991]. Prior to this, subduction related to the closure of the pre-Atlantic affected the

whole of the UK, but this activity ceased around  $\sim 350$  Ma. There are no evident seismic velocity anomalies beneath the UK which might indicate a vestigial thermal imprint from these tectonic episodes or a deep lithospheric structure whose composition or temperature may be anomalous [Grand, 1994]. It appears, therefore, that the UK is a suitable area to explore for unusual transition zone structure.

To investigate the transition zone's discontinuity structure, we analyze broadband recordings of teleseismic P-wave arrivals. We use receiver function analysis to isolate the P-to-S conversions at the discontinuities,  $P_{410s}$  and  $P_{660s}$ , and to determine discontinuity depths and converted wave strengths. We find normal discontinuity depths compatible with the expectation that there should be no deviation from average properties given the tectonic age of the region. However, the 660-km discontinuity conversion appears to be anomalously weak, which may indicate unusual structure between 410 and 660 km, or unusual properties of the 660 itself.

## Data and Methods

The data are broadband recordings of teleseismic P and PP from a temporary network of nine broadband stations located in northern Scotland and operated for about 14 months, called the RUSH-I project. Figure 1 shows a map of station locations and the earthquakes used. The earthquakes provided 102 records for receiver function analysis. The positions of the interaction points with the 410- and 660-km discontinuities cluster under the northern North Sea, and eastern Atlantic. We used standard frequency-domain water-level deconvolution methods to isolate the P-to-S conversions in the wave field [Langston, 1979; Owens *et al.*, 1984; Ammon, 1991], with a frequency smoothing factor of 5 and a water level of  $10^{-4}$ . The data is noisy due

to the ocean microseisms which are inescapable in the UK, but only exceptionally was notch filtering used to remove noise before deconvolution. The deconvolved traces were then analyzed for appropriate moveout of the phases of interest,  $P_{410s}$  and  $P_{660s}$ , and stacked for analysis. Figure 2 shows a slowness section for the unfiltered receiver functions. The clustering for each event is due to the change in slowness with distance of P and PP over the narrow aperture of the network. The horizontal dashed lines show the predicted arrival times of  $P/PP_{410s}$  and  $P/PP_{660s}$  with slowness (the  $P/PP$  notation indicates the P-to-S conversion is of either P or PP). Clearly, noise obscures individual arrivals. To establish whether the phases are actually present in the data, we sum the receiver functions along the predicted  $P_zs$  moveout curves (for conversions from different depths  $z$ ) to check that the summed trace amplitude maxima occur at the expected lags for the expected depths. This is akin to velocity spectrum stacking used by *Gurrola et al.* [1991], but here we handle it like slant-stacking where the control parameter, rather than being slowness, is  $\Delta t/\Delta p$  or moveout, which has units of degrees for our choice of slowness unit. We show the slant-stacked receiver function traces in Figure 3. While the peak amplitude for the arrival around 42 s, which from inspection of Figure 2 should correspond to  $P/PP_{410s}$ , is at its expected moveout value, the arrival at 65 s,  $P/PP_{660s}$ , is not. When its amplitude peaks, it has the correct time lag, but significantly less moveout than predicted. WKB synthetic [Chapman et al., 1988] for P, PcP and PP, plus the depth phases and 410- and 660-km conversions with the reported CMT focal mechanisms, processed and slant-stacked similarly show interference around the  $P/PP_{660s}$  arrival time from PcP depth phases, which have lower moveout, partly explaining the anomalous stack features around 65 s. However the depth phases stack with the same sign as the  $P/PP_{660s}$

and slightly enhance its amplitude, suggesting that the observed peak position may be early but its amplitude must represent an upper bound for  $P/PP_{660s}$ .

The final processing stage consisted of optionally filtering the receiver functions (using zero phase bandpass filters between 10s-40s and 5s-30s) and transforming the time axes of the receiver functions to depth by calculating the  $P/PP_zs - P/PP$  time lag for each depth  $z$  using the AK135 model [Kennett et al., 1995]. The transformed receiver functions were then stacked by linear summation, and 95% confidence bounds on the stacks were computed from the pointwise variance of the sum.

## Results

Most of the recorded events arrived along easterly back-azimuths, preferentially sampling the northern North Sea region between the Orkney and the Shetland islands (Fig. 1). We found that the receiver function stacks along westerly back-azimuths had a distinctly different character than the eastern ones. For these reasons, we discarded those fewer records from the stacks. The stacks displayed in Figure 4 contain transition zone peaks above the 95% confidence level at 414 km and at 669 km. There is no peak between 500 and 600 km above the 95% confidence level. To estimate the uncertainty in the peak position, we use two further whole-earth velocity models, SP6 [Morelli and Dziewonski, 1993] and IASP91 [Kennett and Engdahl, 1991] to transform time to depth and report the variability in peak position, which yield uncertainties of  $\pm 1$  km in the vicinity of 410, and  $\pm 2$  km in the vicinity of 660. An additional component of the error budget is the variability of the peak's position in the stacks at different frequencies, which is  $\pm 4$  and  $\pm 12$  km for the 410 and 660, respectively. Thus the 410- and 660-km

discontinuity positions are  $414 \pm 5$  and  $655 \pm 14$  km. The 660's position represents the middle of the observed range of positions in the variously-filtered stacks.

The negative peaks flanking the one at 414 km appear to be side-lobe artifacts produced by the deconvolution, so we choose not to interpret them further. The peaks at 643 and 668 km are similar in amplitude and merge with filtering. The larger uncertainty in position, in combination with the improper moveout of this arrival in the unfiltered data makes its identity somewhat uncertain, but it is the only feature between 500 and 700 km above the 95% confidence level.

## Discussion

The observed positions of the 410- and 660-km discontinuities are, within uncertainty, at their standard depths, indicating no displacement of them due to unusual thermal structure. It also suggests that topography on the discontinuities is absent because they are both visible, and small-scale topography tends to render them invisible [van der Lee *et al.*, 1994]. Thus an analysis of converted wave amplitudes seems warranted because extraneous influences are probably minimal.

The  $P/PP_{410s}$  amplitude is  $0.049 \pm 0.27(2\sigma)$  on the unfiltered receiver function stack, and the  $P/PP_{660s}$  amplitude is  $0.029 \pm 0.17(2\sigma)$ , relative to a unit amplitude P arrival on the vertical component. At the 95% confidence level, the  $P/PP_{410s}$  value corresponds to the predicted value for AK135 [Kennett *et al.*, 1995; Montagner and Kennett, 1996] 0.030, at  $6.7 s/^\circ$ , the average slowness of the stacked traces, while  $P/PP_{660s}$  is significantly below the predicted value of 0.051. We therefore consider the  $P/PP_{660s}$  amplitude to be anomalous. To provide a useful characterization for analysis, we work with the amplitude ratio  $P_{660s}/P_{410s}$  which is nearly

constant at 1.66 over the slowness range  $4s/^\circ \leq p \leq 8s/^\circ$  covering most of our observations (Figure 2). The P-to-S conversion occurs at different depths, which contributes a minor amplitude correction factor of 1.11 on account of the impedance difference and 0.95 on account of differential attenuation (using PREM  $Q$  values [Dziewonski and Anderson, 1981]). The observed  $P_{660s}/P_{410s}$  ratio is 0.59 as compared to the ‘‘normal’’ (with corrections) AK135 value of 1.75. If we adopt the AK135  $P_{410s}$  amplitude ratio and the highest  $P_{660s}$  amplitude allowable in the 95% confidence limits, the  $P_{660s}/P_{410s}$  ratio is 1.53.

One way to significantly reduce the ratio is if there is stronger S attenuation between 410 and 660. The travel time of an S wave with a slowness of  $6.7s/^\circ$  (the average slowness in our observations) is 50 s. To reduce amplitudes to between 0.35-0.90 in this brief time interval at a period of 5 s requires  $Q$  to be 30-70, which is 2-5 times lower than PREM values for the transition zone.

Another possibility is that the wavespeed jumps in AK135 at 660 km might be wrong. *Estabrook and Kind* [1996] found no underside  $P_{660}P$  reflections in waveform stacks of global data and concluded there was no jump in the Lamé parameter  $\lambda$  or seismic parameter  $\Phi$  there. *Shearer and Flanagan* [1999], using long-period  $SS$  precursors, found a smaller jump in S wavespeeds and density than AK135, and *Castle and Creager* [2000], using  $S_{660}P$ , found a larger S jump but smaller density jump as well. Adopting *Estabrook and Kind's* [1996] constraints on  $\lambda$  and  $\Phi$  and *Castle and Creager's* [2000] S jump yields extremely large  $P_{660s}/P_{410s}$  ratios  $> 2.8$ , which we feel is unlikely to be compatible with our observations. However, *Shearer and Flanagan's* [1999]  $\Delta V_s$  of 0.27 km/sec, in combination with *Estabrook and Kind's* [1996] constraints, yields a  $P_{660s}/P_{410s}$  ratio of 1.27 which

is within our observational uncertainty. Thus jumps in P, S, and  $\rho$  of 1.9, 4.8 and 4.8%, respectively, as compared to the AK135 values of 5.8, 6.2, and 8.2%, would satisfy our observations.

An alternative way to decrease  $P_{660s}$  is by broadening the 660-km discontinuity. We use the methods to parameterize the  $(\text{Mg, Fe})_2\text{SiO}_4 = (\text{Mg, Fe})\text{O} + (\text{Mg, Fe})\text{SiO}_3$  transformation described in *Helfrich and Wood* [1996] to explore broadening this transition by calculating frequency-dependent P-to-S conversion coefficients. The method broadens the mixed-phase region over a finite depth interval, and uses extrapolation of the AK135 velocity profiles above and below the 660 to derive the elastic properties of the mixed-phase region. By widening transition interval to 13 km we can reduce calculated  $P_{660s}/P_{410s}$  ratio to 1.53 at  $6.7 s/^\circ$  slowness 5 s period. This is minimal perturbation to 660 properties, arising from the use of AK135 410 values and the extreme  $P_{660s}$  amplitude allowable in the 95% confidence bounds. If we use the observed  $P_{660s}$  amplitude, the required broadening is 30 km, and if we additionally use the observed  $P_{410s}$  amplitude the broadening is 35 km. The possible profiles through the transition region are shown in Figure 4.

These results suggest that complexities in 660-km discontinuity structure exist away from areas of thermal perturbations such as subduction zones. Three mineralogical factors potentially capable of changing 660 structure are  $\text{MgSiO}_3$  ilmenite, the garnet-perovskite transition, and water in ringwoodite. Ilmenite is stabilized at low temperatures [*Vacher et al.*, 1998] uncharacteristic of the normal mantle under the UK, so we reject this idea. Ferric iron increases the velocity jump at the 660 by enhancing Al uptake into perovskite, eliminating the gradient zone below 660 normally due to the dissolution of Al-bearing majoritic garnet into perovskite [*Wood and Rubie*, 1996; *Wood*, 2000]. This ef-

fect would strengthen  $P_{660s}$ , opposite to what we observe. Water, however, partitions more strongly into ringwoodite, extending its stability and broadening its multiphase region by up to 0.5 GPa [*Higo et al.*, 2001]. Lateral variations in water content above the 660 therefore appears to be a feasible way to reduce the  $P_{660s}$  conversion, but a more rigorous thermodynamic analysis, beyond the scope of this contribution, is required to establish how extensive the broadening could be.

## Conclusions

Receiver function analyses of P-to-S conversions for teleseismic P and PP arrivals under the UK reveal visible conversions from the 410, but a weak corresponding conversion from the 660 and no visible conversions from the vicinity of 520 kilometers. The inferred discontinuity depths are  $414 \pm 5$  and  $655 \pm 14$  km, which are nominal. The  $P_{660s}/P_{410s}$  amplitude ratio predicted by AK135 is  $\sim 1.6$ , whereas we observe ratios of  $\sim 0.59$ , suggesting a significant weakening of the 660 conversion without a change in its depth. Allowing the amplitude ratio to vary within its 95% confidence bounds leads to a range of possible changes to transition zone structure that include stronger attenuation (2-5 times PREM) and broadening of the 660 km discontinuity. We find that decreasing the jumps at the 660, or broadening it to a transition region about 13 km thick would yield reduced amplitudes compatible with those that we observe. Lateral variation in transition zone water content is one way to broaden the 660.

## Acknowledgements

The deployment relied on the help and goodwill of many individuals. We thank the people and landowners of Bettyhill, Scotland, for their warm hospitality, those in Syre, Altnaharra,

Rogart and Airdens for support, the Orkney Council for access to the site on Hoy, Al Munro for overseeing the Bonar Bridge site, and the late Jack Irvine of Hoy for his “can-do” attitude. NERC grant GR9/04304 funded the research work, and the NERC Geophysical Equipment Pool provided instruments and logistical support. We thank Bernie Wood and Tine Thomas for helpful discussions.

## References

- Ammon, C., Isolation of receiver effects from teleseismic *P* waveforms, *Bull. Seismol. Soc. Am.*, *82*, 2504–2510, 1991.
- Bina, C. R. and B. J. Wood, Olivine-spinel transitions: Experimental and thermodynamic constraints and implications for the nature of the 400-km discontinuity, *J. Geophys. Res.*, *92*, 4853–4866, 1987.
- Castle, J. C. and K. C. Creager, Local sharpness and shear wave speed jump across the 660-km discontinuity, *J. Geophys. Res.*, *105*, 6191–6200, 2000.
- Chapman, C., C. Jen-yi, and D. G. Lyness, The WKBJ seismogram algorithm, in *Seismological Algorithms*, edited by D. Doornbos. Academic Press, New York, 1988.
- Deuss, A. and J. H. Woodhouse, Seismic observations of splitting of the mid-transition zone discontinuity in the Earth’s mantle, *Science*, *294*, 354–357, 2001.
- Dziewonski, A. M. and D. L. Anderson, Preliminary reference earth model, *Phys. Earth Planet. Inter.*, *25*, 297–356, 1981.
- Estabrook, C. H. and R. Kind, The nature of the 660-kilometer upper mantle discontinuity from precursors to the PP phase, *Science*, *274*, 1179–1182, 1996.
- Grand, S. P., Mantle shear structure beneath the Americas and surrounding oceans, *J. Geophys. Res.*, *99*, 11591–11621, 1994.
- Gurrola, H., J. B. Minster, and T. Owens, The use of velocity spectrum for stacking receiver functions and imaging upper mantle discontinuities, *Geophys. J. Int.*, *117*, 2504–2510, 1991.
- Harris, A. L., The growth and structure of Scotland, in *Geology of Scotland*, edited by G. Y. Craig, pages 1–24. Geological Society of London, London, 1991.
- Helfrich, G. and B. J. Wood, 410 km discontinuity sharpness and the form of the olivine  $\alpha - \beta$  phase diagram: Resolution of apparent seismic contradictions, *Geophys. J. Int.*, *126*, F6–11, 1996.
- Helfrich, G. R., Topography of the transition zone seismic discontinuities, *Rev. Geophys.*, *38*, 141–158, 2000.
- Higo, Y., T. Inoue, T. Irifune, and H. Yurimoto, Effect of water on the spinel-postspinel transformation in  $Mg_2SiO_4$ , *Geophys. Res. Lett.*, *28*, 3505–3508, 2001.
- Ita, J. and L. Stixrude, Petrology, elasticity, and composition of the mantle transition zone, *J. Geophys. Res.*, *97*, 6849–6866, 1992.
- Kennett, B. L. N. and E. R. Engdahl, Travel-times for global earthquake location and phase identification, *Geophys. J. Int.*, *105*, 429–565, 1991.
- Kennett, B. L. N., E. R. Engdahl, and R. Buland, Constraints on seismic velocities in the Earth from traveltimes, *Geophys. J. Int.*, *122*, 108–124, 1995.
- Langston, C. A., Structure under Mount Rainier, Washington, inferred from teleseismic body

- waves, *J. Geophys. Res.*, *84*, 4749–4762, 1979.
- Montagner, J.-P. and B. L. N. Kennett, How to reconcile body-wave and normal-mode reference earth models, *Geophys. J. Int.*, *125*, 229–248, 1996.
- Morelli, A. and A. M. Dziewonski, Body wave traveltimes and a spherically *P*- and *S*-wave velocity model, *Geophys. J. Int.*, *112*, 178–194, 1993.
- Owens, T. J., G. Zandt, and S. R. Taylor, Seismic evidence for an ancient rift beneath the Cumberland Plateau, Tennessee: A detailed analysis of broadband telsesismic *P* waveforms, *J. Geophys. Res.*, *89*, 7783–7795, 1984.
- Shearer, P. M. and M. P. Flanagan, Seismic velocity and density jumps across the 410- and 660-km discontinuities in Earth’s upper mantle, *Science*, *285*, 1545–1548, 1999.
- Simmons, N. A. and H. Gurrola, Multiple seismic discontinuities near the base of the transition zone in the Earth’s mantle, *Nature*, *405*, 559–562, 2000.
- Vacher, P., A. Mocquet, and C. Sotin, Computation of seismic profiles from mineral physics: the importance of the non-olivine components for explaining the 660 km depth discontinuity, *Phys. Earth Planet. Inter.*, *106*, 275–298, 1998.
- van der Lee, S., H. Paulssen, and G. Nolet, Variability of P660s phases as a consequence of topography on the 660 km discontinuity, *Phys. Earth Planet. Inter.*, *86*, 147–164, 1994.
- White, R. S. and D. McKenzie, Magmatism at rift zones - the generation of volcanic continental margins and flood basalts, *J. Geophys. Res.*, *94*, 7685–7729, 1989.
- Wood, B. J., Phase transformations and partitioning relations in peridotite under lower mantle conditions, *Earth Planet. Sci. Lett.*, *174*, 341–354, 2000.
- Wood, B. J. and D. C. Rubie, The effect of alumina on phase transformations at the 660-kilometer discontinuity from Fe-Mg partitioning experiments, *Science*, *273*, 1522–1524, 1996.
- 
- G. Helffrich, Earth Sciences, University of Bristol, Bristol BS8 1RJ, UK  
 E. Asencio, J. Knapp, T. Owens, Geological Science, University of South Carolina, Columbia, SC 29208, USA
- 
- This preprint was prepared with AGU’s L<sup>A</sup>T<sub>E</sub>X macros v5.01. File ms formatted February 27, 2002.

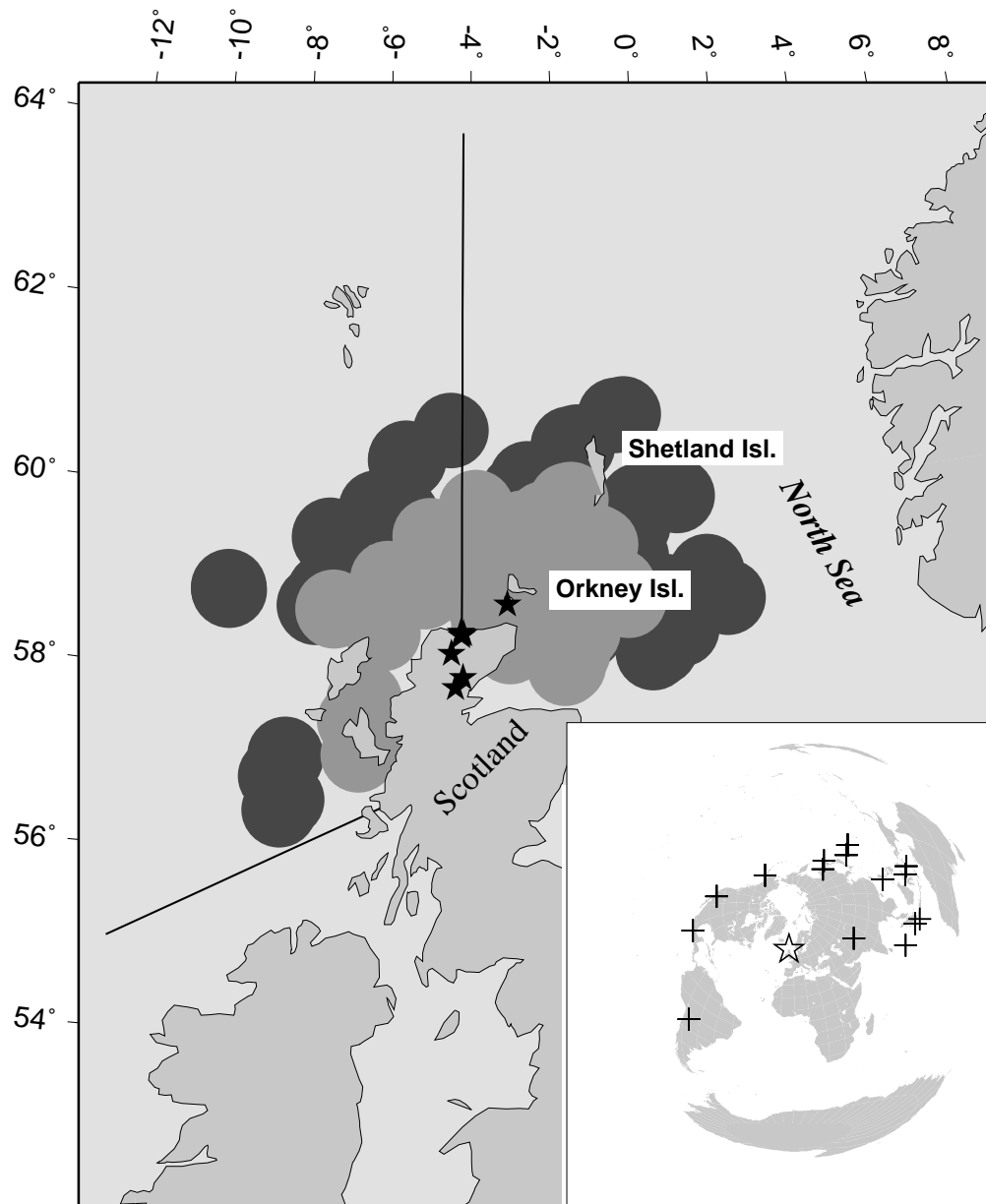


**Figure 1.** Map of RUSH-I network stations in northern Scotland (stars) and the interaction points where upgoing P and PP rays cross the 410- and 660-km discontinuities in the upper mantle (light and darker circular regions). Inset contains azimuthal-equidistant map of earthquakes used (crosses) and network location (star). There is no path coverage to the southeast of the network. Receiver functions for events in the outlined sector with western back-azimuths had a distinctly different character than eastern events, so were not analyzed.

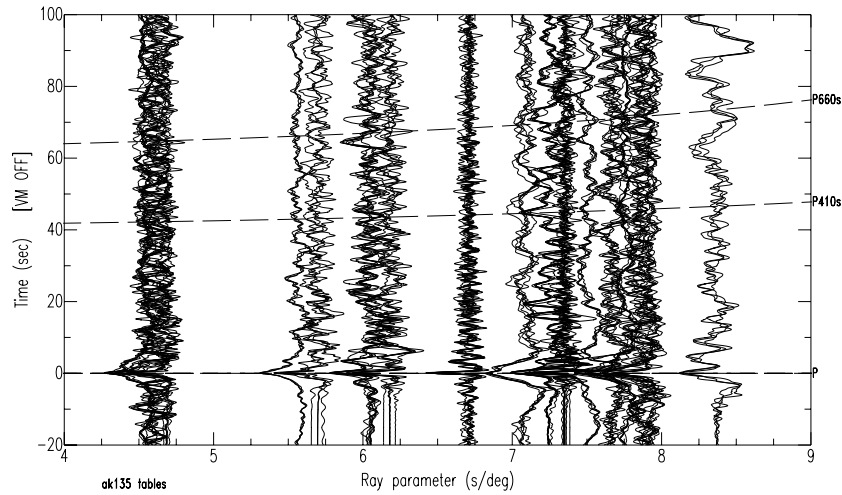


**Figure 2.** Record section of radial component receiver functions ordered by slowness of the incoming P-wave. Clusters of traces represent records of one event, with slightly different slownesses due to  $dp/d\Delta$  of P or PP. Dashed lines are calculated moveout with slowness of  $P_zs$ , a P-to-S conversion at depth  $z$ , using AK135 wave speeds.

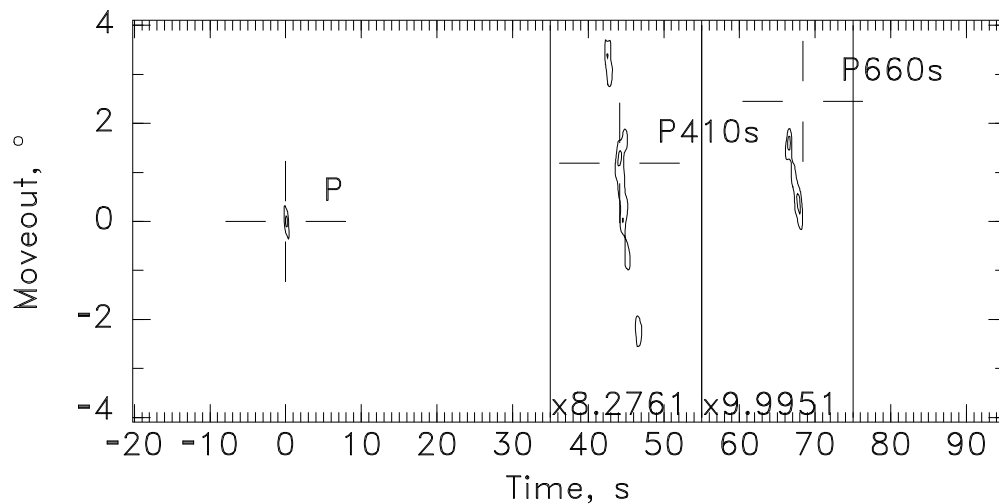


**Figure 3.** Slant-stack of unfiltered receiver function traces for identification of P-to-S converted phases. The horizontal axis is time, and the vertical axis is travel time divided by horizontal slowness, or moveout, with units of degrees for our choice of slowness unit. Contours indicate amplitude maxima in slant-stacked traces (0.8 and 0.95 of maximum), and crosshairs indicate the expected moveout and time of  $P_{410s}$  and  $P_{660s}$  conversions.  $P_{410s}$  is clear, but the  $P_{660s}$  moveout is low and early due to interference by PcP depth phases; agreement with predicted  $P_{660s}$  moveout improves with bandpass filtering. Vertical lines delimit time intervals where stack amplitudes are magnified by the numerical factor given at the bottom.

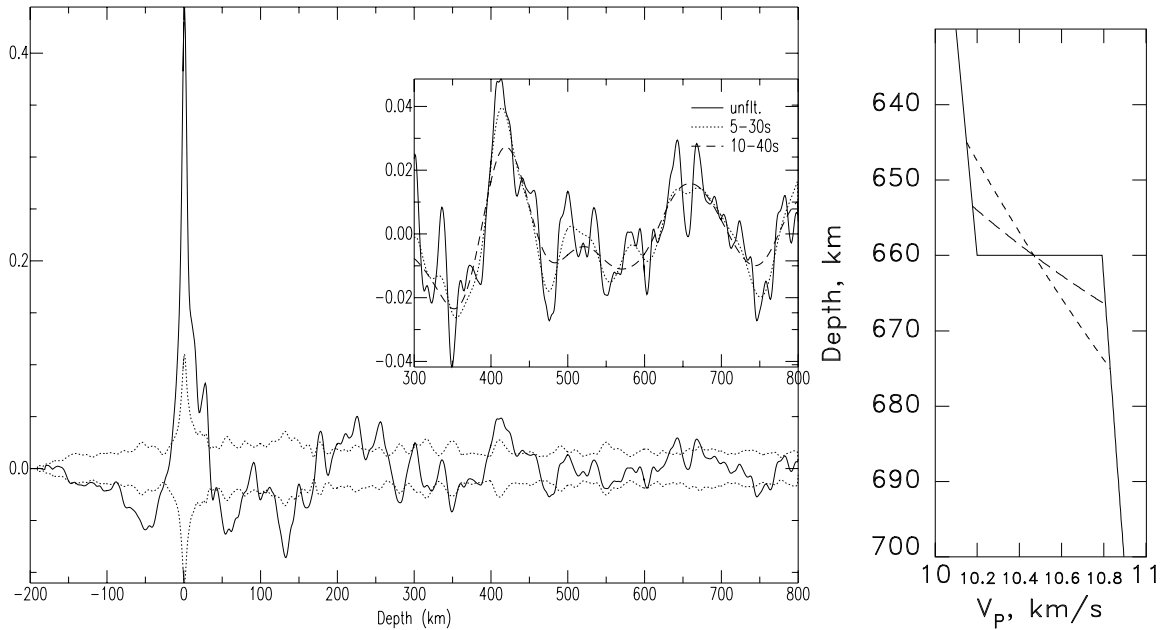


**Figure 4.** Linearly stacked, depth-migrated radial receiver functions (solid line) and 95% confidence level (dashed lines) estimated by the pointwise variance of the stacks, are in the left panel. Inset shows 300-800 km depth interval and unfiltered and filtered receiver function traces (5-30s and 10-40s zero-phase bandpass filters). Right panel shows the P-wavespeed profile through the transition region. Curvature is due to low- and high-pressure phase mixing via the lever rule [Helfrich and Wood, 1996]. Short-dashed line matches amplitudes derived from a pessimistic assessment of  $P_{660s}/P_{410s}$  amplitude uncertainty (30 km), whereas the long-dashed matches the most optimistic assessment (13 km).